International Journal of Environmental Science and Technology (2026) 23:39
https://doi.org/10.1007/s13762-025-06912-5

ORIGINAL PAPER

Adsorptive performance of cobalt/manganese oxide modulation via mechanochemical synthesis route on toxic congo red removal

M. Buğdaycı[1,2] · N. Kanmaz[1] · P. Demircivi[1] · S. Baslayici[2]

Received: 27 June 2025 / Revised: 18 September 2025 / Accepted: 21 September 2025 / Published online: 26 November 2025

Abstract

In this study, cobalt oxide (Co_3O_4) and manganese oxide (MnO) were employed for synthesizing hybrid oxides CoMnOx using a ball-milling technique and evaluated for congo red (CR) removal. The prepared adsorbent samples were characterized by using XRD, SEM–EDX, BET/N_2, FT-IR, and XPS to determine their structural, morphological, and chemical properties. Adsorption studies were carried out to optimize the parameters of adsorbent dosage, time, pH, temperature and different water matrices. The obtained results demonstrated that CoMnOx2 exhibited the highest adsorption capacity of 218.54 mg g^{-1} following the Langmuir model. Kinetic studies revealed that adsorption reached equilibrium at 300 min and was supported by the Elovich model, meaning that chemical interactions were dominant. Adsorption process was exothermic and spontaneous at low temperatures. Despite the presence of anions and cations in the water medium, it showed effective removal. CoMnOx2 maintained stable performance for five cycles and also performed well in removing different pollutants.

Keywords Congo red · Adsorption · Cobalt oxide · Manganese oxide · Ball-milling

Introduction

Water is one of the most basic needs of all living things (humans, animals, and vegetables) to survive. Eliminating the factors that pollute water is of great importance for the sustainability of the life cycle, one of these pollutants is synthetic dyes (Oladoye et al. 2021; Lade et al. 2015; Mahmoodi et al. 2018). These materials are widely utilized in many industries such as textile, solvents, leather, petroleum, food, cosmetics, paint, pigments, rubber, plastic, paper, printing, pesticides, wood preservation chemicals and the pharmaceutical industry (Adam et al. 2021; Dadfarnia et al. 2015; Mohajershojaei et al. 2015; Katheresan et al. 2018; Hosseini et al. 2019). The removal of pollutants that are used in such a wide range of sectors has become the subject of many studies in recent years (Oladoye et al. 2022; Mahmoodi 2013). Over the last 25 years, dyes and heavy metals have become a significant problem for water resources (Mandal et al. 2021). Methylene blue removal was successfully achieved with metal-based adsorbents in the study conducted by Senthilnathan et al. (Marcelino and Amorim 2019). Dyes and pigments are the pollutants most commonly found in the wastewater of food, clothing and pharmaceutical industries. These structures are highly carcinogenic and mutagenic. Because pigments are harmful wastes that are unlikely to biodegrade (Costa et al. 2020; Oladoye et al. 2022; Gadore et al. 2023).

Among the substances that pollute water is the congo red (CR) dye, which has a very high toxicity. This material, also known as 1-naphthalenesulfonic acid, 3,3′-(4,4′-biphenylenebis(azo)) bis(4-amino-) disodium salt, is a synthetically produced anionic dye. CR is used in the polymer, paint and textile industries. Approximately 7000 articles have been published in the last quarter century on the removal of this material, which shows the intense interest in the subject (Jasim and Salman 2024). In these scientific studies for CR removal, photocatalytic methods (Prabhakar et al. 2024), oxidation (Tehrani et al. 2024), membrane systems (Harja et al. 2022a), adsorption methods and catalytic systems were examined. The adsorption method for dye removal is a tremendous water cleaning technique that

Editorial responsibility: Samareh Mirkia.

✉ N. Kanmaz
nergizkanmaz@gmail.com

[1] Faculty of Engineering, Department of Chemical Engineering, Yalova University, 77200 Yalova, Turkey

[2] Vocational School, Construction Technology Department, Istanbul Medipol University, 34810 Istanbul, Turkey

stands out with its molecular separation feature. In addition, the adsorption method offers many advantages with its fast process time, easy applicability and low economic requirement (Raval et al. 2016). In the case of adsorption studies, structures consisting of clay, activated carbon, biochar, metal–organic frameworks and metal oxide composites were used as adsorbents and their effects on Congo red removal were investigated (Al-Tohamy et al. 2022; Rasilingwani et al. 2024). The practical application of Congo Red removal in industrial wastewater treatment has significant environmental and operational implications. Efficient adsorption or catalytic degradation of this azo dye can substantially reduce the release of toxic and recalcitrant organic pollutants into aquatic ecosystems, mitigating potential ecological and human health risks. In industrial settings such as textile and dyeing facilities, the integration of effective adsorbents or advanced oxidation catalysts allows for continuous treatment of effluents, lowering chemical oxygen demand (COD) and color intensity while facilitating compliance with regulatory discharge standards. Moreover, the recyclability and stability of the adsorbent or catalyst are crucial for economic feasibility, as frequent replacement or regeneration can increase operational costs. Consequently, optimizing removal efficiency, treatment time, and material reusability is essential for implementing sustainable and scalable solutions for Congo Red-contaminated wastewater in real-world industrial contexts (Oladoye et al. 2022; Karadirek et al. 2024; Al Ajmi et al. 2024). Among these adsorbents, metal oxides stand out with their high adsorption capacities, chemical-thermal stability, functional surface properties, ability to form various composites, reasonable prices, easy accessibility, and effectiveness in removing toxic materials and heavy metals (Avornyo and Chrysikopoulos 2024). The high adsorption capacity of metal oxides comes from their high surface area and reactive surface groups. In this way, they provide more intense binding with pollutants and their interactions are efficient. The high adsorption capacity of metal oxides comes from their high surface area and reactive surface groups. In this way, they provide more intense binding with pollutants and their interactions are efficient. In addition, metal oxide composites do not show any decomposition by preserving their structures in a wide pH and temperature spectrum. Thus, they can be easily used in processes requiring high temperature and abrasion service conditions. In addition, due to the ability of metal oxides to be composite with other adsorbents, their adsorption capacity and the variety of toxic substances they can remove increase. Metal oxide structures appear as effective adsorbents against heavy metals and pollutants in a wide spectrum thanks to the variable bonding regions on their surfaces (Keshta et al. 2024; Agravat et al. 2024; Sharma et al. 2021; Sachin et al. 2023).

Metal based adsorbents have attracted considerable attention in adsorption technologies due to their unique physicochemical properties, such as high surface area, tunable porosity, and abundant active sites that facilitate strong interactions with pollutant molecules. Their surface chemistry, often enriched with hydroxyl groups, enables efficient binding through electrostatic attraction, hydrogen bonding, or surface complexation, thereby enhancing adsorption selectivity and capacity. Moreover, the ability to modify metal oxides into nanostructured or composite forms significantly improves their adsorption efficiency, regeneration potential, and stability under varying environmental conditions. These characteristics make metal oxide-based adsorbents promising candidates for the removal of a wide range of contaminants, including dyes, heavy metals, and organic pollutants, thus underscoring their critical role in advancing adsorption-based water treatment technologies (Lafi et al. 2016; Fouda-Mbanga et al. 2024; Akçamlı and Şenyurt 2021).

The negative factors that can be considered in the use of metal oxide-based adsorbents can be listed as the high energy requirement of the synthesis methods, the inability to provide homogenization due to agglomeration of powders and the high raw material cost (Şenyurt et al. 2021). However, the absence of any heating process in the mechanical alloying method used in this study eliminates the need for high energy requirements. In addition, as a result of the contact of the high-energy balls used in the method with the powders, the balls first merge and then break apart with the impact in the process. This increases the surface area of the material and has a positive effect on the adsorption capacity. In addition, as a result of the planetary milling process, the charge is mixed homogeneously and shows the same effect everywhere (Dapson 2018; Mohd Aamir Khan et al 2025). Accordingly, composites synthesized by mechanical alloying have eliminated the aforementioned disadvantages of metal oxide structures.

According to the literature, there is no study in which congo red removal is performed by using manganese oxide—cobalt oxide composites. Previous reports have demonstrated the use of other bimetallic oxides such as MnFe and CoFe for dye removal, showing good adsorption performance. However, the Co–Mn binary oxide system provides unique advantages, including dual functionality, strong redox activity, and synergistic interactions between Co and Mn, which can significantly enhance adsorption efficiency. To the best of our knowledge, Congo Red removal by CoMnOx composites has not been reported, underscoring the novelty of this study. In addition, these two oxide structures were first transformed into dual functional composites by using the mechanical alloying method in this study. The obtained samples were analysed by XRD, SEM–EDX, BET/N_2, XPS and FTIR techniques to determine their crystalline, surface, morphological and chemical structures. Congo red is a carcinogenic and mutagenic pollutant used intensively

in different industries and its removal from wastewater is of great importance. The large number of publications on this subject reveals the currency of the subject. In this study, a new material was proposed as an adsorbent for the removal of congo red and all the details of the process were examined with deep sensitivity. In addition to the effects of adsorbent dosage, time, pH, temperature and different water environments, the reusability of the adsorbent and its removal performance in different pollutants were investigated within the scope of the study.

Materials and methods

Materials

NaOH, NaCl, $CaCl_2$, $MgNO_3$, $ZnNO_3$, KNO_3, Na_2SO_4 were obtained from Merck. Congo red (Fig. 1), MnO (99.9%), Co_3O_4 (99.9%), HCl (fuming, 37%), doxycycline hyclate, levofloxacin, rhodamine-b, orange (II) sodium salt and methylene blue were supplied from Sigma-Aldrich. All chemicals were in analytical purity.

CoMnOx synthesis by ball-milling

The ball milling synthesis of cobalt–manganese oxide composites can, in principle, be scaled up for industrial applications in Congo Red removal. Although energy consumption is a notable consideration due to prolonged milling times, process optimization—such as reducing milling duration, using energy-efficient mills, and employing renewable energy sources—can enhance sustainability. Moreover, the high stability and recyclability of the composite minimize material replacement and secondary waste, supporting environmentally sustainable wastewater treatment at larger scales.

Varying the milling time and ball-to-powder ratio (BPR) significantly affects the physical properties of Co–Mn oxide ($CoMnO_x$) composites. Increasing the milling time generally leads to finer particle sizes and higher surface areas due to increased mechanical activation and repeated particle breakage. However, excessively long milling can cause particle agglomeration, reducing accessible surface area and altering pore structure. Similarly, a higher BPR generally promotes more efficient particle size reduction and defect formation by increasing collision frequency and impact energy, which can increase surface area and create mesopores. Conversely, a BPR that is too high can cause cold welding and densification, reducing porosity. Therefore, careful optimization of both milling time and BPR is essential to obtain $CoMnO_x$ composites with the desired surface area and pore size distribution for efficient adsorption of contaminants such as Congo Red. In this study, initial experiments were performed for 1, 2, 4, 5 and 8 h with varying BPR ratios and the studies were continued with the 5-h experiment, which showed the most optimum adsorption ability.

0.5, 1.0, 1.5 and 2.0 g of cobalt oxide powder (Co_3O_4) was added to 10 g of manganese oxide (MnO) and milled in a ball mill at 500 rpm for 5 h. Stainless steel balls with a diameter of 0.5 cm at 10 times the mass were placed on the powders during milling. At the end of the milling time, the powders were sieved to separate from the balls, kept at 105 °C for 2 h and were ground in a mortar. Adsorbents were labelled as CoMnOx1, CoMnOx2, CoMnOx3 and CoMnOx4 according to the increasing mass amount of Co_3O_4 from 0.5 to 2.0. The preparation steps of adsorbents are illustrated in Fig. 2. Ball milling parameters (time, speed, ball-to-powder ratio) directly influence crystallite size and surface area, thereby tuning adsorption performance. Compared with hydrothermal or co-precipitation methods, the mechanochemical route avoids solvents and heating, offering higher energy

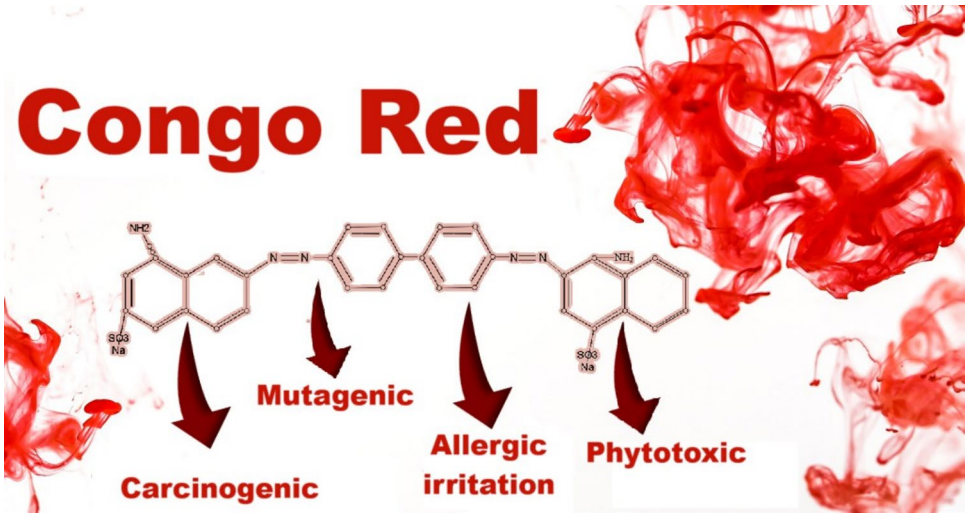

Fig. 1 Congo red dye chemical structure and toxic characteristics

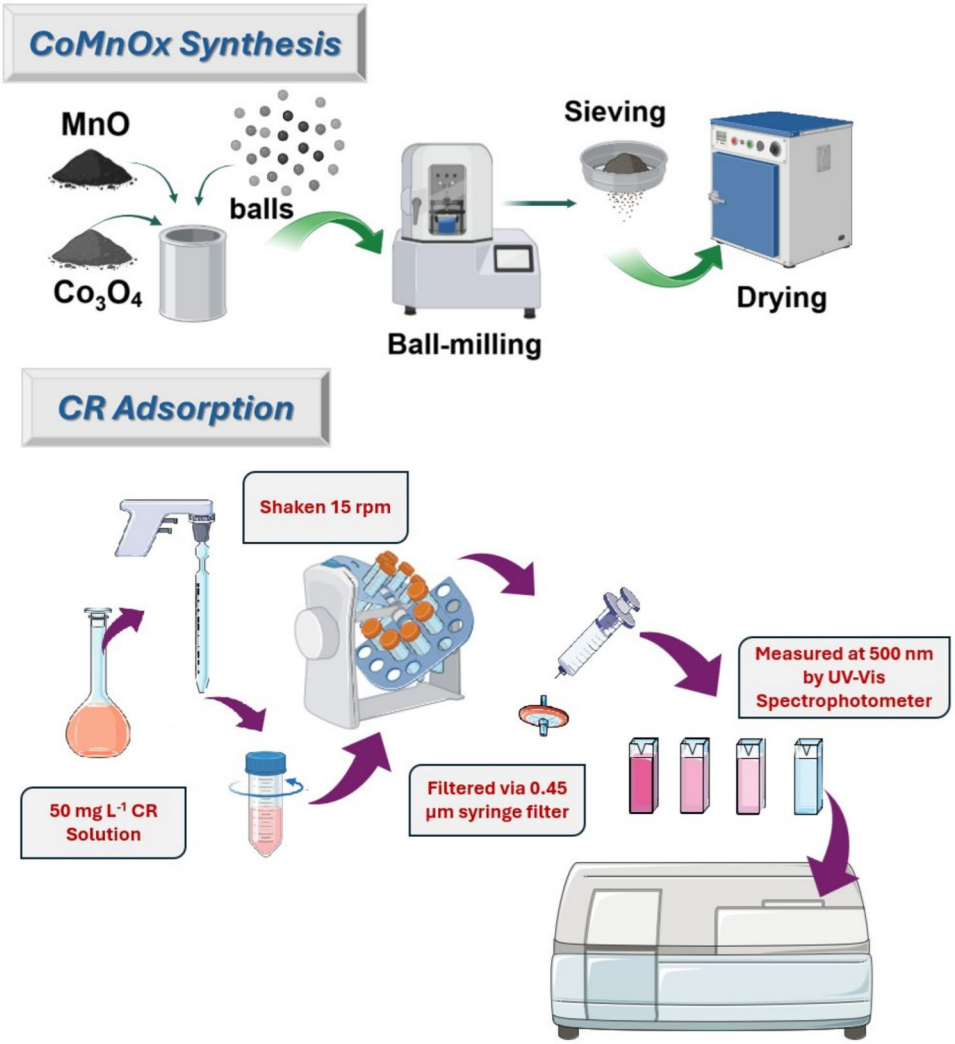

Fig. 2 CoMnOx sorbent synthesis route and CR adsorption steps

efficiency. Its simplicity and scalability further underline the sustainability advantages of this method. In this study, the cost estimation for synthesizing a MnO–Co_3O_4 composite via planetary ball milling was conducted for a bulk-scale production of 1 kg. Considering raw material prices of MnO at 0.01 USD/g and Co_3O_4 at 0.10 USD/g, the total material cost amounts to approximately 110 USD. Energy consumption of a 0.5 kW planetary mill operating for 5 h corresponds to 2.5 kWh, which translates to an electricity cost of roughly 0.38 USD assuming a unit price of 0.15 USD/kWh. Therefore, the total estimated cost for producing 1 kg of the MnO–Co_3O_4 composite is around 310 USD, demonstrating that planetary ball milling remains a relatively cost-effective method for preparing bulk quantities of mixed metal oxide powders under laboratory-scale conditions.

Characterization techniques

X-Ray diffractometer (PANalytical X-Pert3 Powder) was utilized to identicate crystalline structures. The functional groups of the sorbents were determined by Fourier Transform-Infrared Spectroscopy (FT-IR, Perkin Elmer Spectrum 100) in the range of 4000–650 cm^{-1} wavenumber. The surface morphology of fresh and CR loaded sorbents were obtained from scanning electron microscopy-energy dispersive X-ray spectroscopy (SEM–EDX, Carl Zeiss 300VP). The surface area properties of the sample were carried out using the BET technique using a high vacuum analyzer (Quantachrome Quadrasorb SI). The electronic states of the metal oxide sorbent was determined by X-ray photoelectron spectroscopy (XPS; Thermo Scientific K-Alpha X-ray photoelectron spectrometer).

Batch studies

10 mL of 70 mg L^{-1} CR solution was added to 15 mL plastic tubes over different amounts (3–100 mg) of sorbent and shaken at 15 rpm for 24 h by using rotator. In the kinetic experiments, 10 mL of 50 mg L^{-1} CR solution was shaken with the optimum amount of adsorbent for times ranging from 15–360 min. CR solutions prepared at different pHs (pH:5.5–11.0) were studied for the system under the same conditions. It was investigated at 298 K-328 K to examine the temperature effect on CR removal process. To explore the water matrix effect, 50 mg L^{-1} CR solutions were prepared using tap water, lake water and seawater and 50 mg L^{-1} of Ca^{2+}, Na^{+}, Mg^{2+}, Zn^{2+}, NO_3^{-}, SO_4^{2-} solutions. The removal stability of the adsorbent was investigated by regenerating the adsorbents with 10 mL ethyl alcohol after each cycle, then drying and conducting CR adsorption again. 10 mL of 50 mg L^{-1} of other types of contaminants which were rhodamine-b (λ_{555nm}), methylene blue (λ_{665nm}), orange-II (λ_{485nm}), levofloxacin (λ_{290nm}) and doxycycline (λ_{354nm}) were conducted. After the adsorption process, the suspension was filtered by using a 0.45 µm syringe filter to determine CR concentration. The concentration of the solution was measured at 500 nm wavelength in UV–Vis Spectrophotometer. The adsorption capacity and adsorption ratio were calculated as in Eqs. 1 and 2.

$$q_{e,t} = \frac{(C_o - C_{e,t}) \times V}{m} \quad (1)$$

$$\text{CR Removal } (\%) = \frac{(C_o - C_{e,t})}{C_o} x100 \quad (2)$$

where $q_{e,t}$, C_o, $C_{e,t}$, V and m are adsorption capacity at equilibrium and at t time (mg g^{-1}), initial CR concentration, CR concentration in equilibrium and at t time (mg L^{-1}), the volume of CR solution (L) and the adsorbent mass (g), respectively.

Results and discussion

Characterization of samples

The crystal structure of the inorganic samples consisting of MnO and Co_3O_4 and the determination of the phases formed were first analysed. Figure 3 (a) shows the XRD results of mechanically alloyed samples. The change in the amount of cobalt oxide added to MnO from 0.5 to 2 g caused an increase in the intensity of the peaks. This showed that the increased cobalt oxide encouraged alloying and provided the formation of more intense peaks. In addition, the same phases were obtained in all cobalt oxide amounts, the MnO phase was visualized as a clubs, Beta MnO_2 phase as a circle, CoO as a diamond and Co_3O_4 phase as a spades. When the mixing ratios were taken into consideration, it was seen that the main phase was MnO as it should be, and it was determined that cobalt contents were included in the structure at every ratio. Here, cobalt oxide structures appear in cubic form, while manganese oxide structures are in tetragonal form. The Co_3O_4 structure has the Fd-3 m space group symmetry and is located at the [111], [220], and [310] positions in the cubic lattice. The CoO structure has the F-43 m space group symmetry and is located at the [111], [200], and [220] positions in the lattice. MnO_2 has the tetragonal structure and has the P 42/m n m space symmetry. Peaks

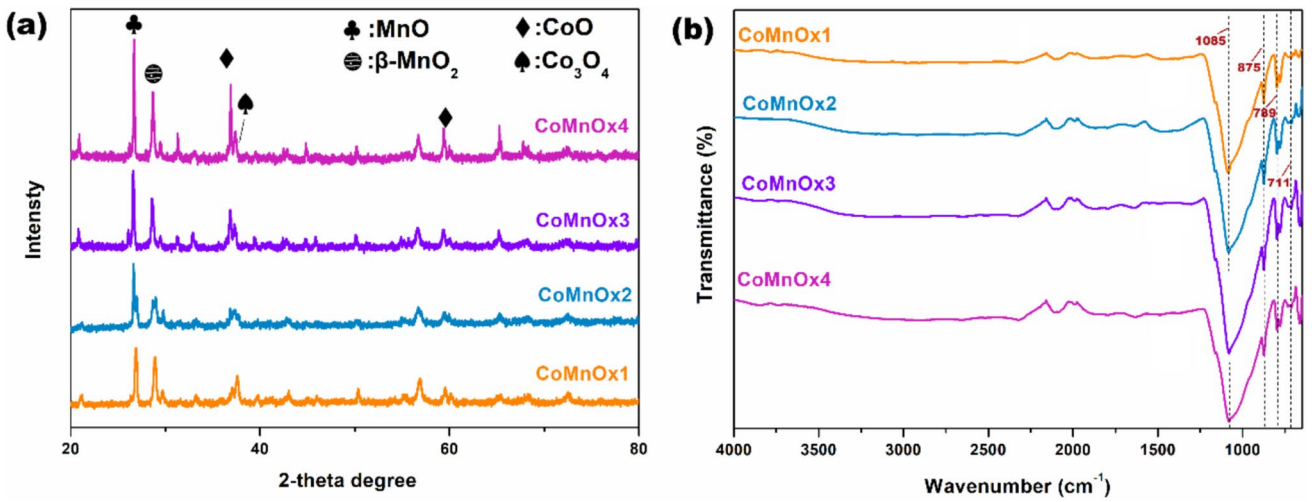

Fig. 3 **a** XRD patterns (JCPDS: Co_3O_4(01–078-1970), CoO (01–075-0419), MnO_2(98–000-5737), MnO (00–005-0673) and **b** FT-IR spectra of sorbents

in the XRD diagram appear at the [110], [011], and [020] points of the tetragonal lattice. Finally, MnO gives peaks at the [100], [110], and [111] points without showing any space geometry.

FT-IR spectra of CoMnOx samples (Fig. 3 (b)) confirm the presence of metal oxides with their characteristic peaks. Accordingly, FT-IR findings with parallel characteristics to Fig. 3 (a) were obtained. Similar peaks were obtained in all mixture ratios, and an intensification of peak intensities was observed in CoMnOx3 and CoMnOx4 ratios. This shows that the increasing amount of cobalt oxide in the mixture promotes alloying, as observed in XRD findings. On the other hand, the sharp peak observed around 1085 cm^{-1} confirms the presence of metal–oxygen (M–O) bonds and indicates Co-Mn–O bonding. The peaks at 875 cm^{-1} and 789 cm^{-1} are attributed to the typical stretching modes of Co_3O_4. The low-frequency peak observed at 711 cm^{-1} corresponds to the characteristic vibration mode of Mn–O bonds. The FT-IR data show that CoMnOx adsorbents were successfully prepared for dual functionalities of binary oxides and that these structures provide active metal oxide sites that favour the adsorption of congo red molecules.

SEM analyses were performed to determine the microstructure and chemical composition of the powders and the 500 X and 20 k X magnification results of the CoMnOx2 sample are shown in Fig. 4 (a and b), respectively. In addition, the mapping and EDX results of the sample are shown in Fig. 4 (c and d). According to the SEM results, it was seen that cobalt oxide phases were attached and combined on the MnO matrix structure and according to the EDX results, no structure other than Mn, Co and oxygen was observed. When the scaling of the SEM micrographs is considered, it is easily seen that the powder size is below 20 microns as a result of mechanical grinding. This plays an important role in increasing the adsorption capacity of the powders. The mapping results show that cobalt-based structures are concentrated in certain regions and positioned on the homogeneously distributed Mn-based structure and that oxygen is distributed equally everywhere. These results confirm that the optimized milling parameters (5 h milling time and selected BPR) promoted a balance between particle refinement and avoidance of agglomeration, resulting in improved surface area and accessible adsorption sites.

N_2 adsorption/desorption analysis was employed to characterise the surface properties of CoMnOx2. The BET isotherm graph obtained for the sample is presented in Fig. 5 (a) and the curve indicates Type IV isotherm. Type IV is generally characteristic for mesoporous materials and is also consistent with a typical hysteresis loop, which increases dramatically when the P/P_o value is above 0.9, as illustrated in the graph. This implies that CoMnOx2 has a significant amount of mesopores. According to surface area calculations, the specific surface area of CoMnOx2 was found to be 11.01 $m^2\ g^{-1}$, which is very valuable in supporting the adsorption performance of the material. The pore size distribution presented in Fig. 5 (b) reveals an average pore diameter of 23.71 nm. The pore volume was calculated as 0.06 $cm^3\ g^{-1}$ and these results indicate that CoMnOx2 is a suitable material for adsorbing large organic molecules such as congo red (1.4 Å, 9.3 Å and 21 Å) (Miao et al. 2021).

The XPS analysis results of CoMnOx2 powder are displayed in Fig. 6 (a-d). As seen in Fig. 6 (a), the broad scan spectrum clearly demonstrates the characteristic binding energy peaks for the elements Co 2p, Mn 2p and O 1 s. The high-resolution spectrum of the Co 2p region (Fig. 6 (b)) gives Co $2p_{3/2}$ peaks at 780.0 eV and Co $2p_{1/2}$ peaks at 795.0 eV, indicating the + 2 and + 3 oxidation states of Co. The spectrum in the Mn 2p region (Fig. 6(c)) shows that Mn is in the + 2 oxidation state with binding energies of Mn $2p_{3/2}$ at 642.0 eV and Mn $2p_{1/2}$ at 653.8 eV. In addition, the O 1 s peak (Fig. 6 (d)) was observed around 530.0 eV, which confirms that oxygen is present in the oxide form in the CoMnOx2 structure. These XPS analysis results reveal that both Co and Mn metal centres in CoMnOx2 are in oxide form and present active adsorption sites. In this context, it is an important parameter explaining the high efficiency of CoMnOx2, an oxide structured hybrid, in the adsorption of congo red. Notably, Co^{2+}/Co^{3+} redox couples provide strong affinity toward sulfonate groups of CR, while Mn^{2+} species facilitate electrostatic interactions with azo groups, and the balanced surface composition enables synergistic binding. This indicates that the surface composition and oxidation states of Co and Mn play a critical role in governing adsorption efficiency.

Adsorption isotherm and adsorbent dosage effects

The adsorption performances of four different samples were compared to determine the highest capacity hybrid. Accordingly, 10 mL of 70 mg L^{-1} CR solutions were shaken with 0.003–0.1 g adsorbent and adsorption capacities (q_e) were calculated over the estimated concentrations of the filtrates (C_e). Afterwards, Langmuir, Freundlich, Temkin and Dubinin-Radushkevich isotherm model equations (Eqs. (S1-4)) presented in the supplementary file were applied to the C_e-q_e data obtained. Figure 7 (a-d) shows the experimental and model isotherm curves of each sample, while Fig. 7 (c) shows the collective experimental isotherm curves of the four adsorbents. Langmuir curves showed the best matching to the experimental equilibrium data.

The isothermal parameters calculated from the isotherm model equations, the correlation coefficients (R^2) giving the model fits and the chi-squared (χ^2) results analysing the differences between the experimental and expected data from the model are tabulated in Table 1. Correlation coefficients were compared, and it was concluded that monolayer

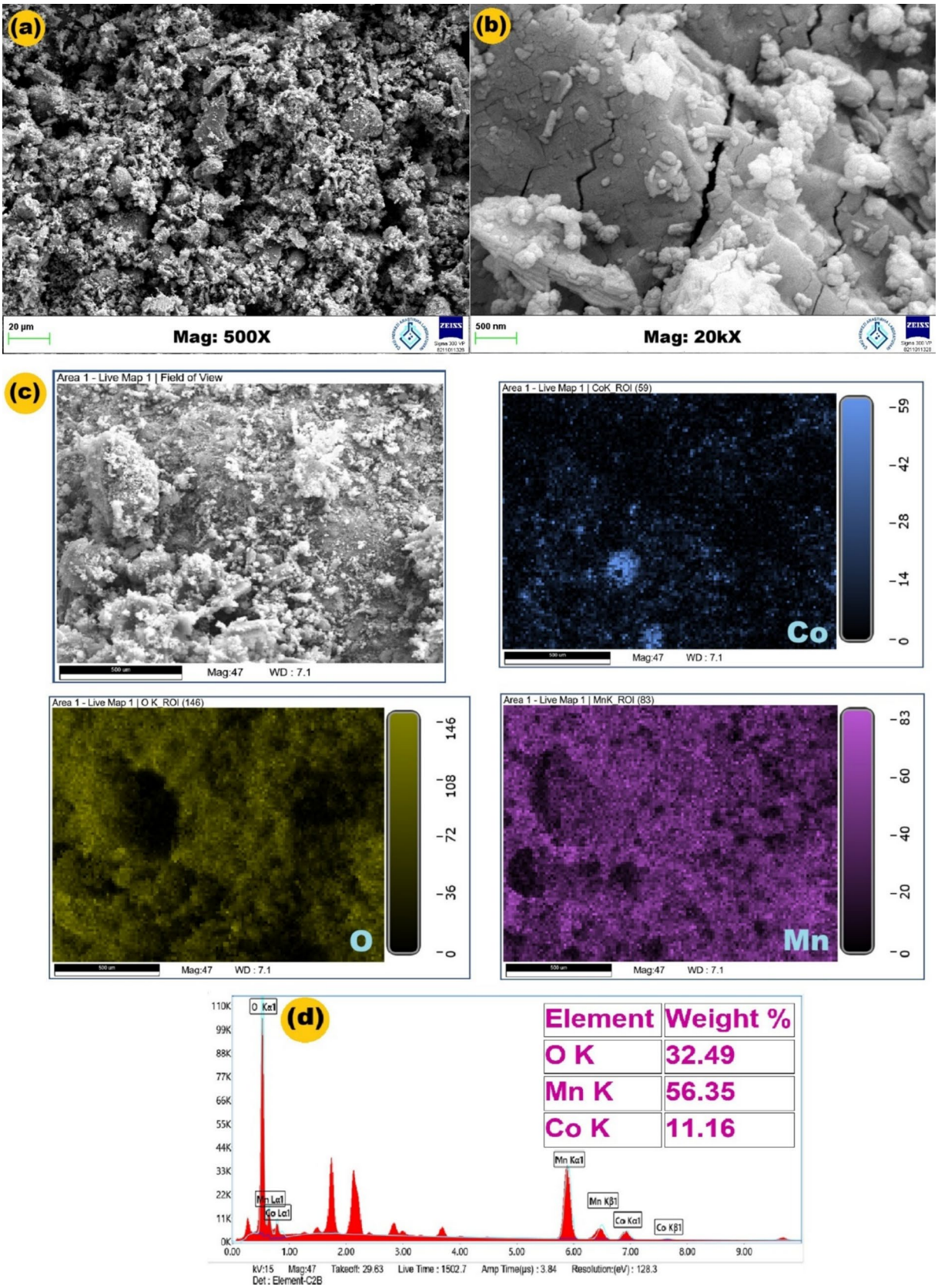

Fig. 4 SEM micrographs of CoMnOx2 with **a** 500X and **b** 20kX, **c** elemental mapping and **d** EDS spectrum

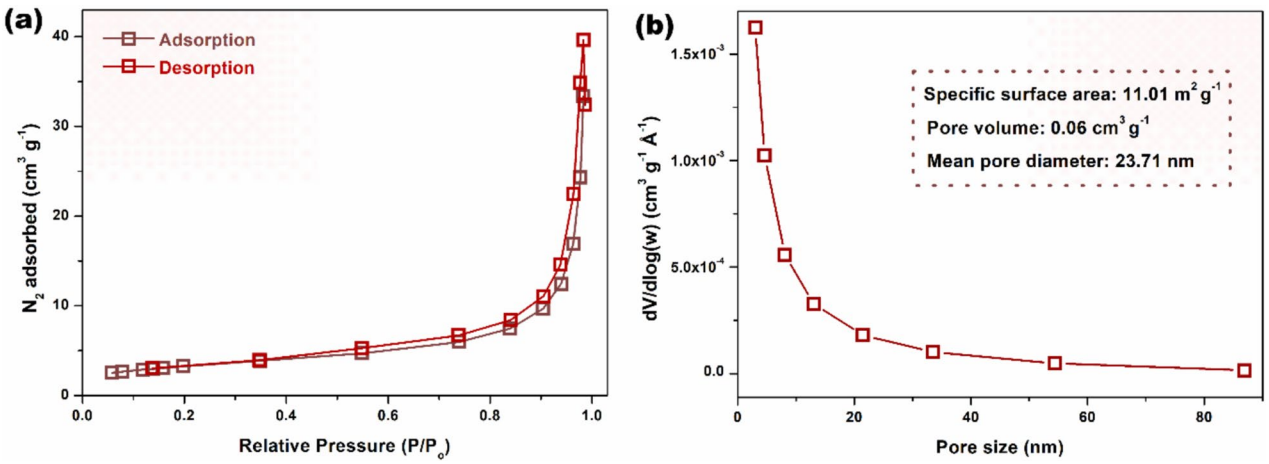

Fig. 5 BET isotherm surface analysis of CoMnOx2

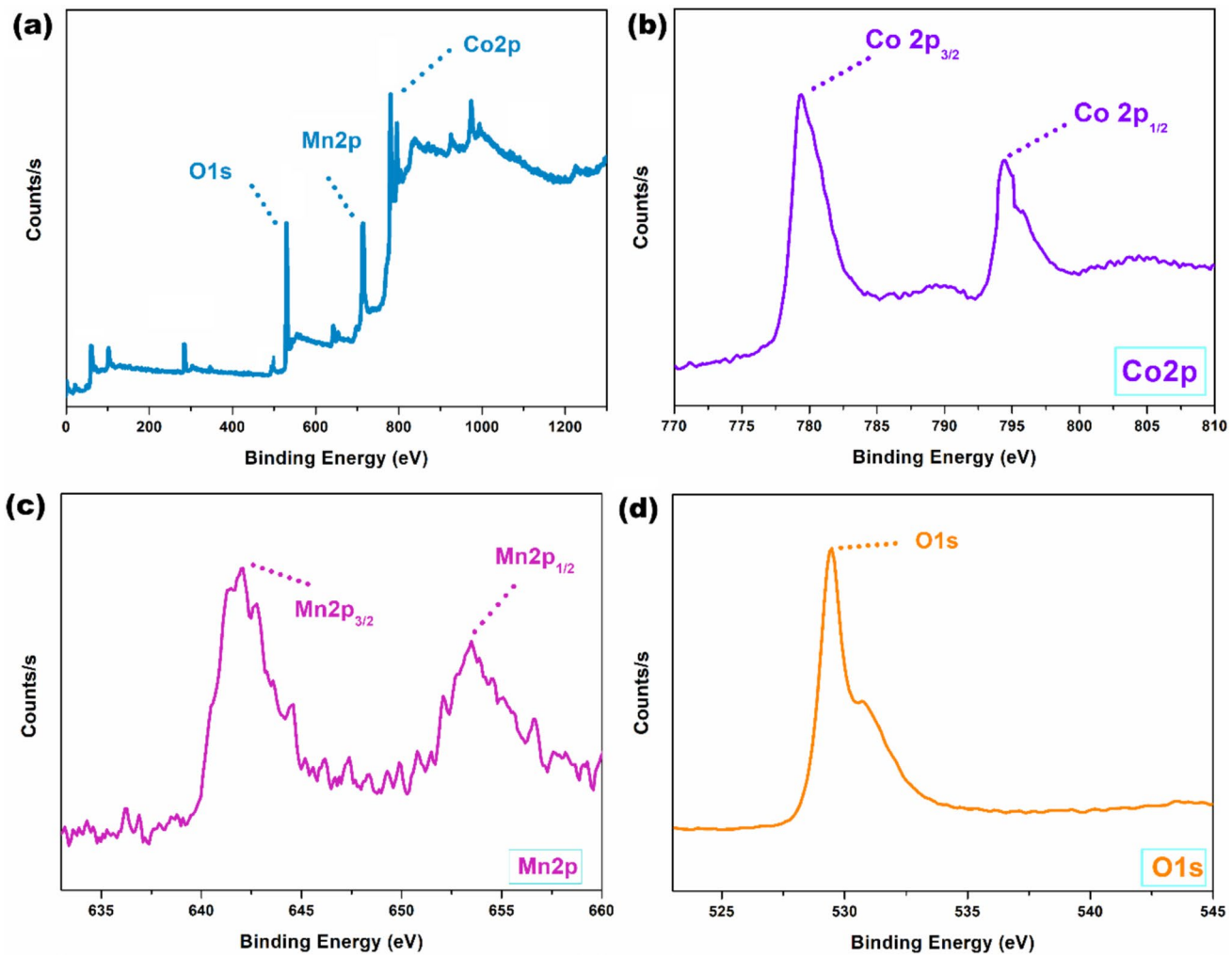

Fig. 6 XPS analysis of CoMnOx2 sample

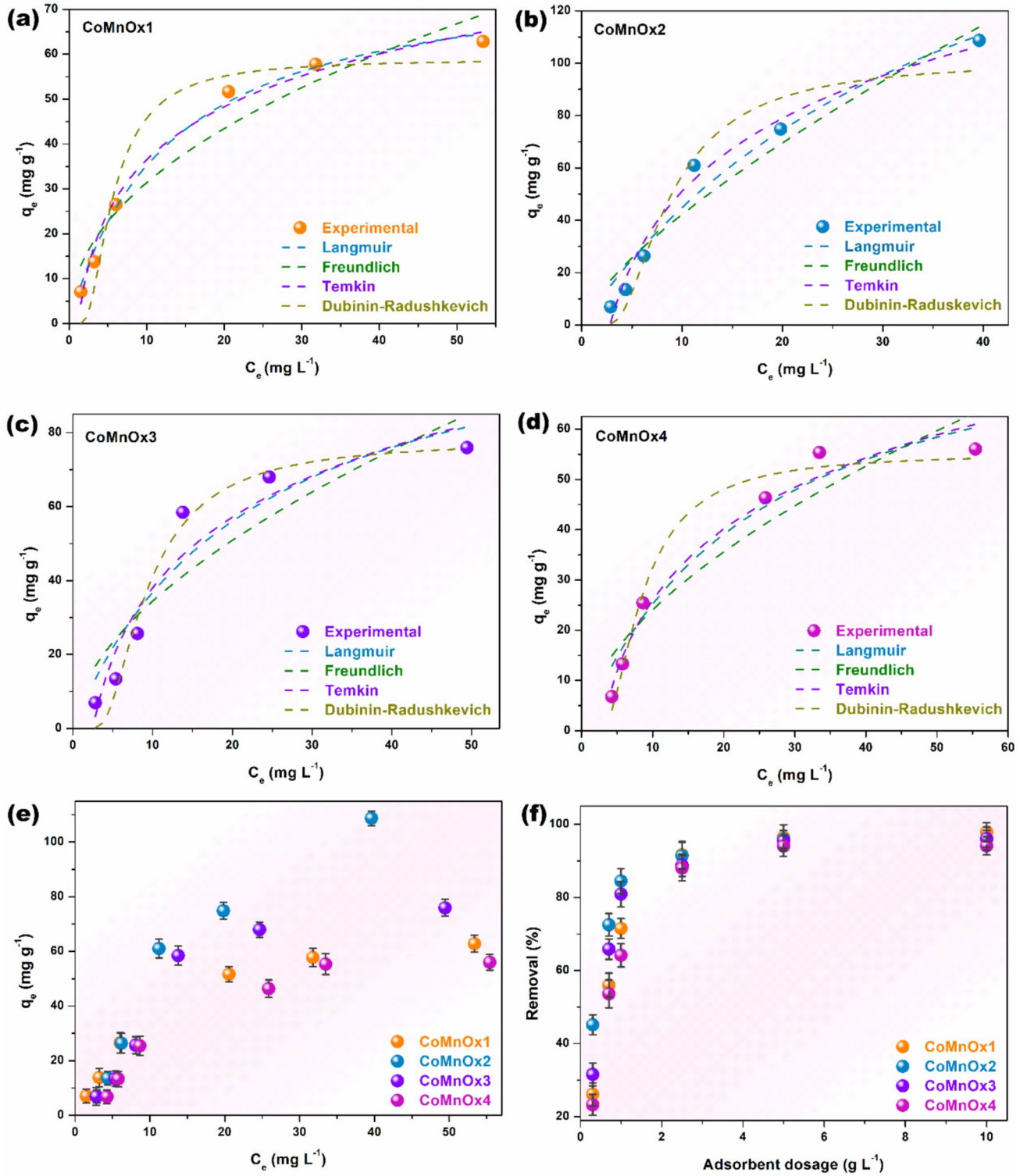

Fig. 7 Isotherm model fitting curves and adsorbent dosage of CoMnOx sorbents

Langmuir model was the most suitable. It is observed that when the monolayer adsorption capacities were compared, the distribution was as follows: CoMnOx2 > CoMnOx3 > CoMnOx4 > CoMnOx1. In these four different samples, different doping ratios were used to determine the optimal ratio at which Co_3O_4 could promote dye adsorption. CoMnOx2, containing 1 g of Co_3O_4, appeared as a ratio containing both the best adsorption performance achieved by

Table 1 Isothermal coefficients of CR adsorption onto sorbents

Models	Parameters	CoMnOx1	CoMnOx2	CoMnOx3	CoMnOx4
Langmuir Isotherm	q_{max} $(mg\ g^{-1})$	79.90	218.54	117.96	87.05
	K_L $(L\ m\ g^{-1})$	0.08	0.02	0.04	0.04
	R^2	0.99	0.98	0.91	0.97
	χ^2	4.26	75.43	102.05	25.69
Freundlich Isotherm	K_F $(L\ g^{-1})$	10.67	8.03	9.38	6.56
	1/n	0.47	0.72	0.56	0.56
	R^2	0.93	0.92	0.79	0.87
	χ^2	75.45	125.27	182.35	58.45
Temkin Isotherm	K_T $(L\ mol^{-1})$	0.86	0.36	0.39	0.35
	b_T $(J\ mol^{-1})$	145.74	61.62	90.00	121.21
	R^2	0.98	0.96	0.89	0.94
	χ^2	9.38	31.82	77.88	14.53
Dubinin Radushkevich Isotherm	q_{max} $(mg\ g^{-1})$	58.87	101.02	77.73	55.17
	E $(J\ mol^{-1})$	0.13	0.09	0.08	0.09
	K_{DR} $(mol^2\ J^2)$	27.68	62.83	70.32	58.49
	R^2	0.84	0.84	0.90	0.92
	χ^2	33.93	93.37	22.41	10.73

the high MnO content and the optimum Co_3O_4 dual support. The CR adsorption capacity of CoMnOx2 was calculated as 218.54 mg g^{-1} from Langmuir equation. The superior fitting of CoMnOx2 to the Langmuir model suggests that its optimized Co/Mn ratio generates more homogeneous and energetically uniform adsorption sites, favoring monolayer adsorption compared to the other composites. Although the BET surface area of CoMnOx2 is relatively low (11.01 $m^2\ g^{-1}$), its high adsorption capacity (218.54 mg g^{-1}) can be attributed to abundant surface active sites arising from Co/Mn redox couples and oxygen functional groups, which favor strong dye binding rather than surface area-driven physisorption. The value demonstrates a higher performance than many adsorbents consisting of inorganic components (Ammar et al. 2021; Parimelazhagan et al. 2022). The 1/n values obtained from Freundlich equations below 1 point out that CR adsorption is favourable. In addition, the correlation coefficient values for Freundlich model in CoMnOx1 and CoMnOx2 were quite high, indicating the involvement of multilayer interactions in the mechanisms occurring on these two adsorbent surfaces. In Temkin model, it is assumed that the heat of adsorption of the active sites on the adsorbent surface decreases linearly with the surface coverage. In Temkin model, which is highly correlated for each adsorbent, the b_T coefficient, calculating the average of these energies, is the lowest for CoMnOx2, where the surface is covered the most. Taken together, the isotherm results reveal that CoMnOx2 outperforms the other composites due to its optimal Co/Mn ratio, which balances high surface area from MnO with the enhanced redox activity and active site availability introduced by Co_3O_4, leading to superior adsorption affinity toward CR molecules.

The removal percentage of CR for varying adsorbent amount was investigated and the results were given in Fig. 7 (f). By increasing the adsorbent amounts from 0.003 g to 0.1 g, both almost all the CR molecules could be removed, and the lowest adsorbent amount was determined. As can be seen in the figure, it was concluded that CR was removed 95% and above for all four adsorbents with 5 g L^{-1} solid–liquid ratio, in other words 0.05 g of adsorbent. In the following sections, it was continued with this optimized adsorbent amount.

Here is a comparative table of adsorbents (Table 2) used for Congo Red (CR) adsorption, with maximum adsorption capacities (q_{max}).

The comparative evaluation of adsorbents employed for Congo Red removal reveals that PDFe/Al nanocomposites exhibit the highest adsorption capacity (411 mg g^{-1}); however, their applicability remains largely restricted to laboratory-scale studies due to synthesis complexity and cost considerations. In contrast, Nelumbo nucifera biomass sorbent demonstrates relatively low adsorption capacity (1.179 mg g^{-1}) and rapid equilibrium attainment, which highlight their potential for practical water treatment applications. Chitosan-derived materials (CS-ECH), while offering comparatively lower adsorption capacity (34.48 mg g^{-1}), present advantages in terms of biodegradability and environmental compatibility. Carboxymethylated Xhantan Gum adsorbent (182.82 mg g^{-1}) stands out as sustainable and economically viable alternatives. Furthermore, iron oxide/carbon nanocomposites, although exhibiting moderate adsorption performance (140.19 mg g^{-1}), benefit from chemisorption-dominated mechanisms that ensure strong and stable dye binding.

Table 2 Comparative table of adsorbents used for Congo Red (CR) adsorption

Adsorbent material	q_{max}, (mg g^{-1})	References
Chitosan–epichlorohydrin (CS-ECH)	*34.48*	Muedi et al. (2022)
Nelumbo nucifera biomass	*1.179*	Pinheiro et al. (2023)
Fe- and Al-based nanocomposites (PDFe/Al)	*411*	Harja et al. (2022b)
Carboxymetylated Xhantan Gum	*182.82*	Singh et al. (2023)
Magnetic Fe_3O_4-loaded fly ash	*154*	Lu et al. (2022)
Heterophase iron oxide/carbon nanocomposite	*140.19*	Xie et al. (2021)

Adsorption kinetics

To determine equilibrium time of CR adsorption and to evaluate the mass transfer mechanisms of CR molecules to the hybrid adsorbent surface, the suspensions were shaken in the range of 15–360 min. When the time-dependent CR removal performance of CoMnOx2 was explored, it was observed that the adsorption started rapidly, and the system reached equilibrium after 300 min with 97.44% removal rate. Figure 8 (a) shows the change in the percentage of CR adsorption over time, indicating that the active sites on the surface are rapidly filled by CR molecules and the adsorption rate slows down when equilibrium is reached. Although the overall equilibrium time was 300 min, it should be emphasized that the adsorption proceeds very rapidly in the initial stage, which is evident from the steep slope of the adsorption curve in the first 60 min. This indicates that a large fraction of the available sites are occupied within a relatively short time. Similar equilibrium times in the range of 240–360 min have also been reported for CR adsorption onto various modified metal oxide and carbon-based adsorbents in the literature (Kanmaz et al. 2025; Yardımcı and Kanmaz 2025). Therefore, our results are consistent with previously reported studies, and the system can be considered to have a reasonably fast adsorption process at the initial stage, even though full equilibrium requires a longer contact time. In Fig. 8 (b), the fit of the kinetic models (Eqs. (S5-8)) to the adsorption data was analyzed and the best fit was found in the Elovich model, indicating that adsorption is governed by chemical interactions. In Fig. 8 (c), the intraparticle diffusion model reveals that there are three different phases in the adsorption process: fast surface adsorption (Phase-1), intrapore diffusion (Phase-2) and equilibrium phase (Phase-3).

Among the kinetic parameters in Table 3, the k_2 value of the pseudo second order model was calculated as 9.7×10^{-3} g (mg min)$^{-1}$ and the regression coefficient (R^2) of this model

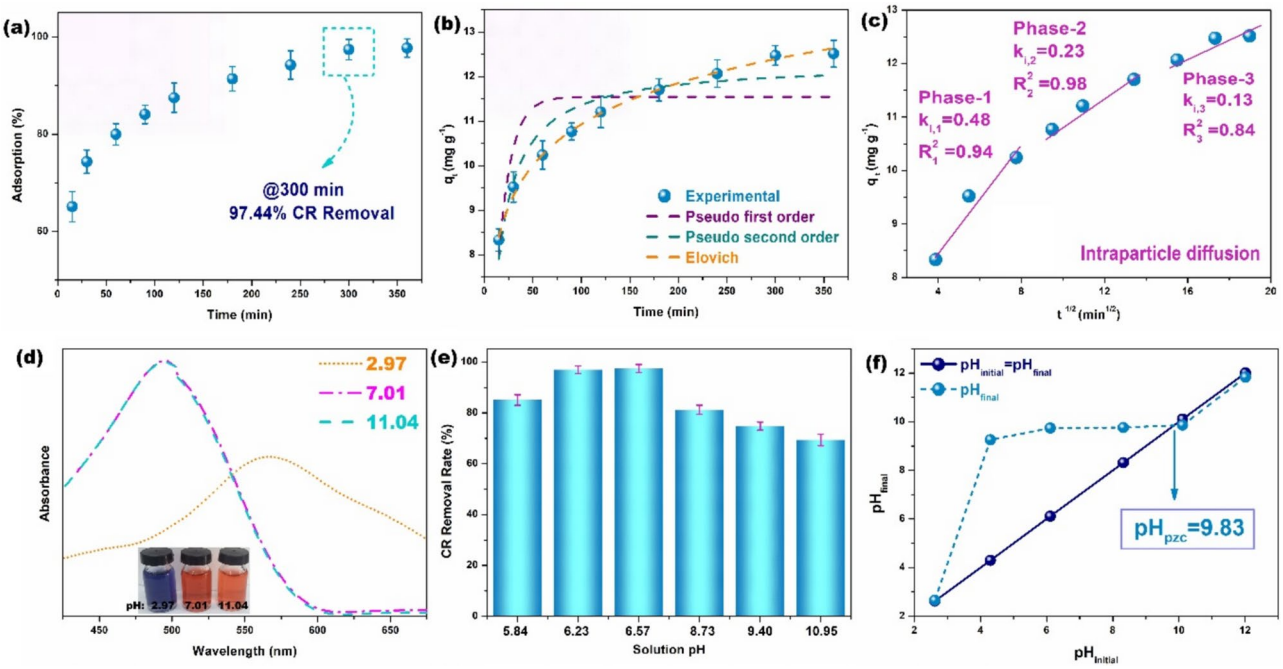

Fig. 8 **a** CR removal percentage by time, **b** experimental and model fitting curves, **c** intraparticle diffusion phase behaviour, **d** CR solution pigmentation in different pHs, **e** pH of solution effect on CR removal and **f** pH_{pzc} plot of CoMnOx2

Table 3 Kinetic model parameters of CR adsorption

Kinetic models	Parameters	Values
Pseudo first order model	k_1 ($L\ min^{-1}$)	7.7×10^{-2}
	q_e ($mg\ g^{-1}$)	11.54
	R^2	0.64
	χ^2	10.30
Pseudo second order model	k_2 ($g\ (mg\ min)^{-1}$)	9.7×10^{-3}
	q_e ($mg\ g^{-1}$)	12.31
	R^2	0.90
	χ^2	3.11
Elovich model	α ($g\ (mg\ min)^{-1}$)	48.67
	β ($mg\ g^{-1}$)	0.75
	R^2	0.99
	χ^2	0.15
Intraparticle diffusion model	$k_{i,1}$ ($g\ mg^{-1}\ min^{-1/2}$)	0.48
	R_1^2	0.94
	$k_{i,2}$ ($g\ mg^{-1}\ min^{-1/2}$)	0.23
	R_2^2	0.98
	$k_{i,3}$ ($g\ mg^{-1}\ min^{-1/2}$)	0.13
	R_3^2	0.84

was found as 0.90, which indicates that adsorption is a process governed by chemical adsorption. The correlation coefficient of the Elovich model was found to be $R^2=0.99$ and when the α and β values calculated from this model are analysed, the initial adsorption rate is many times higher than the desorption rate. This good correlation with the Elovich model suggests that chemisorption dominates the CR removal, consistent with FT-IR analysis that revealed surface oxygen-containing groups (–OH, Mn–O, and Co–O), which provide reactive sites for strong dye–surface interactions. The intraparticle diffusion model (Fig. 8 (c)) shows that adsorption consists of more than one mass transfer phase. Initially, a fast surface adsorption phase was observed, while slower intraparticle diffusion occurred in the second phase. These results reveal that the adsorption is initially fast, but over time the mass transfer rate of CR molecules reaching the pores in the particle decreases.

pH effect on CR removal

Since congo red is an organic pigment affected by pH changes, the colour changes under different pH conditions are shown in Fig. 8 (d). At neutral and alkaline pHs, CR solution exhibits its original red colour and peaks at 500 nm, whereas at acidic pH its colour changes to dark blue and peaks at 570 nm. Figure 8 (e) shows the effect of CR pH on adsorption. The highest adsorption efficiency was obtained at neutral CR solution pH (around pH 6), which can be explained by the strong electrostatic attraction forces formed between the surface and CR molecules at weakly acidic-neutral pH. As the pH increases, the adsorption performance decreases and especially decreases to low levels (69.40%) at pH 10.95. Finally, the zero charge point (pH_{pzc}) of CoMnOx2 was determined as 9.83 in Fig. 8 (f). According to this value, below pH_{pzc}, negatively charged CR molecules are adsorbed more effectively because the surface is positively charged, while above pH_{pzc} the surface becomes negatively charged and the adsorption of CR molecules decreases. While adsorption is efficient below pH 9.83, it decreases above this value due to repulsive forces. These results reveal that adsorption is strongly governed by surface charge and electrostatic interactions. The pH-dependent behavior can be attributed to the interplay between CR speciation and the surface charge of CoMnOx2. At pH around 6, CR exists predominantly in its anionic form, while the point of zero charge ($pH_{pzc}=9.83$) indicates that the adsorbent surface is positively charged, resulting in strong electrostatic attraction and maximum uptake.

Adsorption thermodynamics

In order to investigate the effects of the operating temperature of the process on the adsorption efficiency, shaking was carried out at different temperatures. The obtained Ce and qe values were evaluated as response and Gibbs free energy (ΔG^o), enthalpy (ΔH^o) and entropy (ΔS^o) changes and equilibrium constant (K_d) were calculated by using the equations (S9-11) presented in the supplementary file. The results presented in Table 4 show that the temperature increase has a significant effect on the adsorption capacity in CR adsorption. Based on Kd, the adsorption capacity decreases gradually in the temperature range from 298 to 328 K. The calculated ΔS^o value is negative (-120.47 J mol^{-1} K^{-1}), indicating that the order is decreasing. ΔH^o is -0.035 kJ mol^{-1}, suggesting that the adsorption process is exothermic and low temperatures favour adsorption. ΔG^o values become positive with increasing temperature, showing that the adsorption process becomes less spontaneous and less realisable with temperature. The Van't Hoff plot presented in Fig. 9 (a) confirms that this relationship is linear and that the adsorption mechanism is highly temperature dependent. The decrease in spontaneity at higher temperatures (less negative $\Delta G°$ values) can be attributed to partial desorption driven by enhanced molecular motion, which weakens dye–surface

Table 4 Thermodynamic parameters of CR adsorption

T (K)	K_d	ΔH^o (kJ mol^{-1})	ΔG^o (kJ mol^{-1})	ΔS^o (J mol^{-1} K^{-1})
298	0.77	-0.035	0.65	-120.47
308	0.45		2.03	
318	0.29		3.24	
328	0.21		4.17	

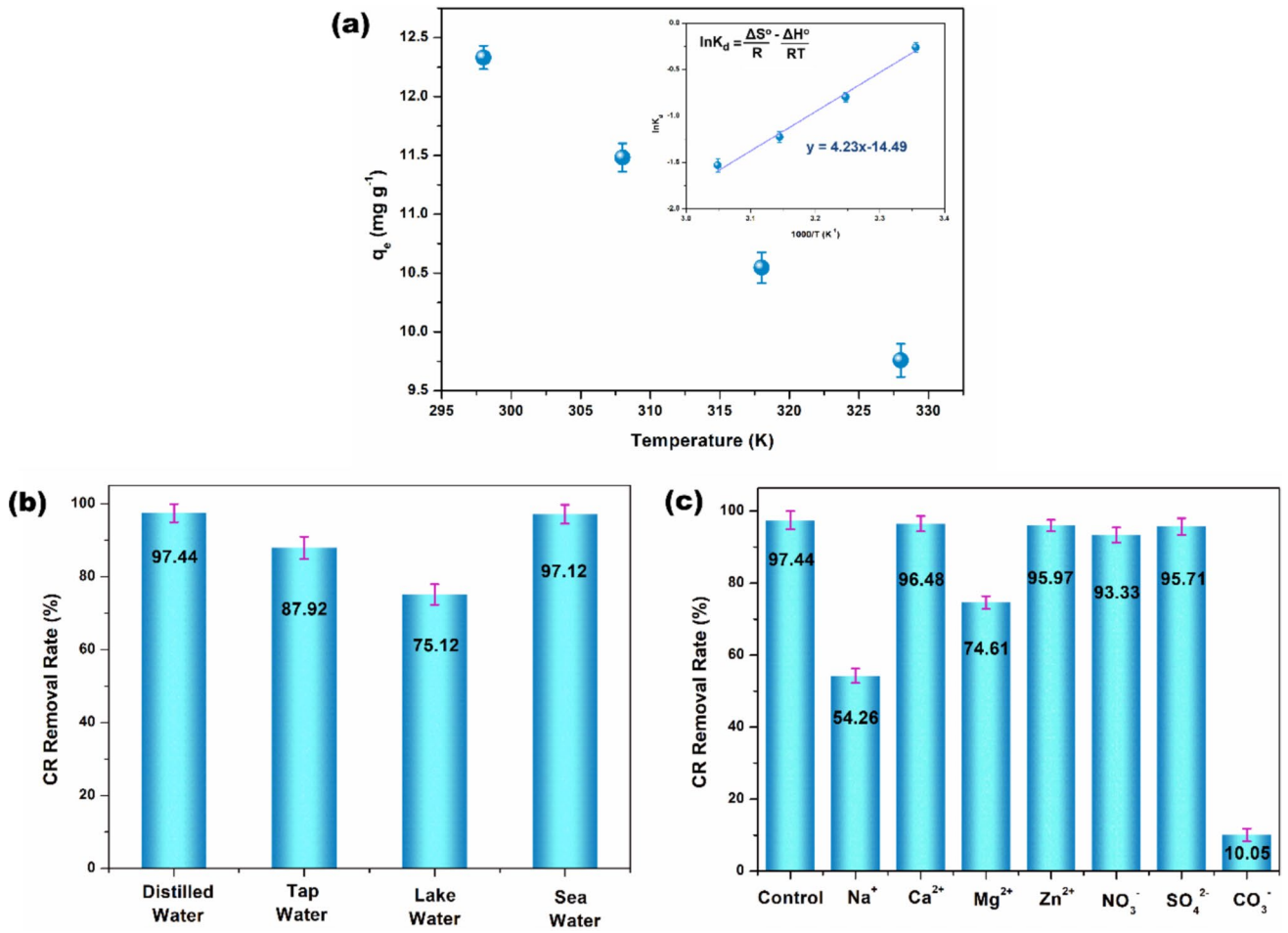

Fig. 9 **a** Van't Hoff graph, **b** different water matrix effects and **c** anion/cation effects

interactions. In real wastewater conditions, this indicates that the material is most effective under ambient temperatures without additional energy input, underscoring its practical applicability.

Water matrix effects

The adsorption performance of CR in different water environments was investigated and the results are presented in Fig. 9 (b). In distilled water 97.44% was obtained, however, adsorption rates in natural waters show a decrease; the removal rate was 87.92% in tap water, 75.12% in lake water, and 97.12% in seawater. According to the data, organic substances and dissolved ions in the composition of the water may affect the adsorption efficiency. Figure 9 (c) shows the effect of anions and cations present in the solution on CR adsorption. In particular, the existence of ions such as Na^+, Ca^{2+} and CO_3^{2-} significantly decreases the adsorption; for example, in the presence of CO_3^{2-} the adsorption rate dropes to as low as 10.05%. This can be attributed to the fact that large ions or high ion concentrations in the solution fill the active sites on the adsorbent surface and inhibit the CR removal (Xu et al. 2024). In the presence of Na^+ ion, CR adsorption was reduced to 54.26%. Na^+ ion is a monovalent cation with a single positive charge and a small, hydrated diameter. It can be concluded that Na^+ has high mobility in solution and quickly reaches the CoMnOx2 surface and competes with CR molecules (Sun et al. 2025). On the other hand, the possible co-existence of heavy metals in real wastewaters may lead to increased competition for active surface areas and alter CR adsorption.

CR adsorption mechanism

CR adsorption mechanism steps were investigated and illustrated in Fig. 10. Despite the relatively low BET surface area (11.01 $m^2\ g^{-1}$), CoMnOx2 exhibited a remarkably high adsorption capacity for CR. This behavior can be attributed to the abundance of chemically active sites provided by Co/Mn redox couples and surface oxygen-containing functional groups (–OH, Co–O, Mn–O), as confirmed by FT-IR and XPS analyses. At the optimum pH (~6.0), CR exists in its

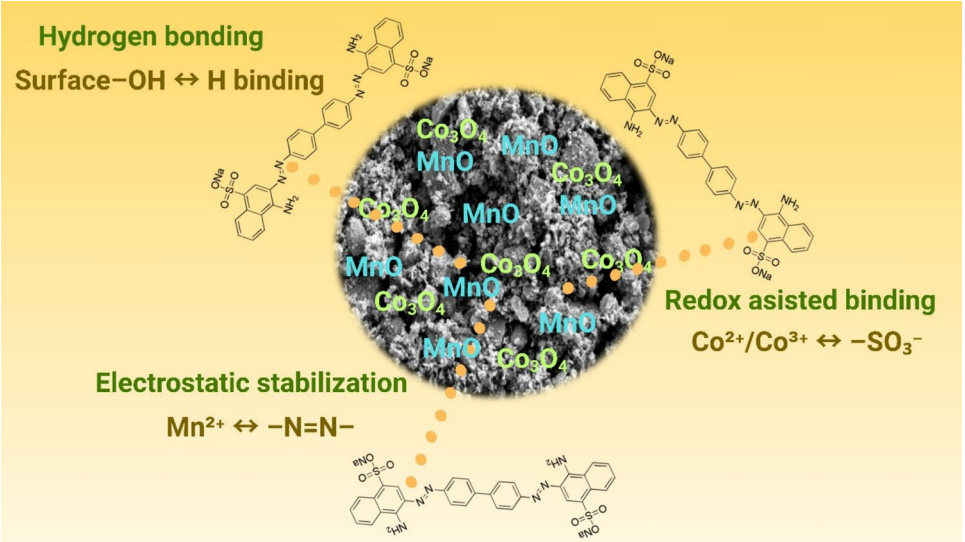

Fig. 10 Possible CR adsorption mechanism on CoMnOx2 surface

anionic form while the CoMnOx2 surface (pH_{pzc} = 9.83) is positively charged, resulting in strong electrostatic attraction. The Elovich kinetic model further indicates the predominance of chemisorption, in line with the surface functionalities observed.

XPS results confirm that Co^{2+}/Co^{3+} redox couples preferentially interact with the sulfonate groups of CR, while Mn^{2+} species stabilize azo groups through electrostatic interactions. Langmuir isotherm fitting suggests that adsorption mainly follows a monolayer process on relatively homogeneous active sites. Thermodynamic analysis demonstrates that adsorption is spontaneous and endothermic at ambient temperatures, but less favorable at elevated temperatures due to partial desorption caused by enhanced molecular motion.

Overall, the adsorption mechanism involves synergistic effects of (i) electrostatic attraction between positively charged Co/Mn oxide sites and anionic CR species, (ii) redox-assisted interactions of Co^{2+}/Co^{3+} couples with sulfonate groups, and (iii) stabilization of azo functionalities by Mn^{2+} sites. This cooperative mechanism explains the high and selective adsorption performance of CoMnOx2 for CR.

Reusability results

The CR removal performance of CoMnOx2 was evaluated over five adsorption cycles, the results are shown in Fig. 11 (a). After each adsorption, the adsorbents were regenerated with ethyl alcohol. While a high removal percentage of 97.44% was obtained in the first use, 78.95% removal was achieved in the fifth cycle. As a result, although CoMnOx2 showed high efficiency in the first few cycles, it experienced a slight loss of performance with successive adsorption

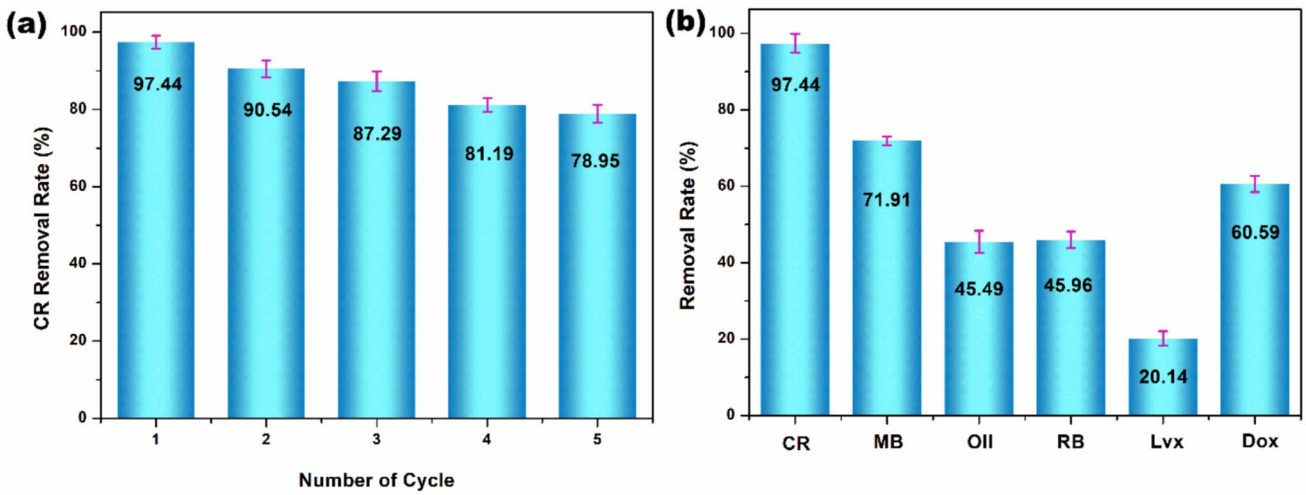

Fig. 11 **a** CR removal stability and **b** different pollutant adsorption performances of CoMnOx2

processes. This decrease may be due to the partial saturation of the active sites on the adsorbent surface and the regeneration process did not fully recover the active sites. Despite being used five times in a row, it had a significantly better CR removal profile than many other sorbents in the literature. This is because it is an inorganic composite material, which gives it a stable matrix [50,51]. The observed decrease in efficiency may also stem from residual CR molecules blocking some of the pores. Moreover, ethanol as a regenerant may not fully desorb strongly adsorbed dye species. The dilute acid/alkali-based regeneration agents, thermal-assisted treatments, or combined solvent strategies could enhance the regeneration efficiency.

Performance in different contaminants

The performance of CoMnOx2 on different organic pollutants under CR optimized conditions (10 mL volume, 50 mg L^{-1} pollutant concentration, natural pH, 5 g L^{-1} adsorbent dose and 298 K temperature) was investigated. The experimental results are illustrated in Fig. 11 (b). While CoMnOx2 effectively removed CR by 97.44%, it was observed that the removal rates of MB, OII and RB were 71.91%, 45.49% and 45.96%, respectively. These results suggest that, based on the structural properties and molecular interactions of the dyes, the surface properties of CoMnOx2 offer different interaction mechanisms in certain pollutants. The high removal with CR indicates that electrostatic interactions and π-π interactions with the surface of the adsorbent strongly occur. The relatively high removal of MB suggests electrostatic attractions between the cationic nature of this dye and negatively charged active sites on the surface.

Concerning antibiotics, the removal rates of Lvx and Dox were 20.14% and 60.59%, respectively. The higher efficiency in Dox shows that hydrogen bonds and other specific interactions with the adsorbent surface occur, while the interactions of the Lvx molecule with the surface are weak. The performance of CoMnOx2 with these pollutants reveals that both electrostatic interactions and physical adsorption are effective, but the chemical and physical interaction capacities of the adsorbent vary according to the pollutant speciation.

Conclusion

This study investigated the performance of CoMnOx hybrid oxides synthesised by ball milling technique for adsorption of toxic congo red dye from aqueous media. XRD, FTIR, SEM–EDX, BET and XPS analyses of the prepared samples were carried out and the successful synthesis was characterised. It was concluded that all adsorbents conformed to the Langmuir monolayer adsorption model. CoMnOx2 containing 1 g Co_3O_4 doped with CoMnOx2 exhibited the highest adsorption performance and the adsorption capacity was found to be 218.54 mg g^{-1}. The process was found to be driven by chemical interactions in accordance with the Elovich kinetic model and the equilibrium time was 300 min. Since it is an anionic dye solution affected by pH, the removal performance decreased in strongly acidic and basic regions. Besides being an exothermic and spontaneous process, it is also a system that can be affected by the presence of components in the water environment. The CoMnOx2 adsorbent confirmed its reusability after five consecutive cycles, maintaining relatively good efficiency with a very small decrease. Finally, the removal performances of different types of organic pollutants were also analysed and showed adsorption efficiency through significant interactions in these different structures. The results of the study underline the potential of CoMnOx materials as cost-effective and environmentally friendly adsorbents and offer a sustainable solution for the removal of hazardous dyes from industrial wastewater.

Supplementary Information The online version contains supplementary material available at https://doi.org/10.1007/s13762-025-06912-5.

Acknowledgment The authors are grateful to the Departments of Chemical Engineering in Yalova University for the use of their facilities for this study.

Author contributions Mehmet Buğdaycı: Conceptualization, investigation, resources, data curation, writing—original draft, writing—review and editing. Nergiz Kanmaz: Data curation, investigation, methodology, writing—original draft, writing—review and editing,

visualization, supervision. Pelin Demircivi: Conceptualization, methodology, resources. Serkan Baslayici: Investigation.

Declarations

Conflict of interest The authors declare no competing interests.

References

Adam AMA, Saad HA, Atta AA, Alsawat M, Hegab MS, Refat MS, Altalhi TA, Alosaimi EH, Younes AAO (2021) Preparation and characterization of new crfeo3-carbon composite using environmentally friendly methods to remove organic dye pollutants from aqueous solutions. Crystals. https://doi.org/10.3390/cryst11080960

Agravat D, Patel SK, Alsalman O (2024) Nanostructured metal-oxide materials for solar energy absorption and conversion for industrial heater applications. Int J Therm Sci 200:108951. https://doi.org/10.1016/j.ijthermalsci.2024.108951

Akçamlı N, Şenyurt B (2021) Fabrication and characterization of in-situ Al3Ni intermetallic and CeO2 particulate-reinforced aluminum matrix composites. Ceram Int 47:21197–21206. https://doi.org/10.1016/j.ceramint.2021.04.122

Al Ajmi ASS, Bosu S, Rajamohan N (2024) Biomass - metal oxide nano composite for the decontamination of phenol from polluted environment - parametric, kinetics and isotherm studies. Environ Res 240:117467. https://doi.org/10.1016/j.envres.2023.117467

Al-Tohamy R, Ali SS, Li F, Okasha KM, Mahmoud YAG, Elsamahy T, Jiao H, Fu Y, Sun J (2022) A critical review on the treatment of dye-containing wastewater: ecotoxicological and health concerns of textile dyes and possible remediation approaches for environmental safety. Ecotoxicol Environ Saf. https://doi.org/10.1016/j.ecoenv.2021.113160

Ammar RB, Labidi A, Salaberria AM, Labidi J, Ayadi S, Abderrabba M (2021) Comparative adsorption of anionic dye congo red and purification of olive mill wastewater by chitin and their derivatives. Desalin Water Treat 220:392–408. https://doi.org/10.5004/dwt.2021.27013

Avornyo A, Chrysikopoulos CV (2024) Applications of graphene oxide (GO) in oily wastewater treatment: recent developments, challenges, and opportunities. J Environ Manage 353:120178. https://doi.org/10.1016/j.jenvman.2024.120178

Costa WD, da Silva Bento AM, de Araújo JAS, Menezes JMC, da Costa JGM, da Cunha FAB, Coutinho HDM, de Paula Filho FJ, Pereira Teixeira RN (2020) Removal of copper(II) ions and lead(II) from aqueous solutions using seeds of *Azadirachta indica* A. Juss as bioadsorbent. Environ Res 183:109213. https://doi.org/10.1016/j.envres.2020.109213

Dadfarnia S, Haji Shabani AM, Moradi SE, Emami S (2015) Methyl red removal from water by iron based metal-organic frameworks loaded onto iron oxide nanoparticle adsorbent. Appl Surf Sci 330:85–93. https://doi.org/10.1016/j.apsusc.2014.12.196

Dapson RW (2018) Amyloid from a histochemical perspective. A review of the structure, properties and types of amyloid, and a proposed staining mechanism for Congo red staining. Biotech Histochem 93(8):543–556. https://doi.org/10.1080/10520295.2018.1528385

Fouda-Mbanga BG, Onotu OP, Olushuyi CI, Nthwane YB, Nyoni B, Zikhona T-N (2024) Application of metallic oxide coated carbon nanoparticles in adsorption of heavy metals and reusability for latent fingerprint detection: a review. Hybrid Adv 6:100248. https://doi.org/10.1016/j.hybadv.2024.100248

Gadore V, Mishra SR, Ahmaruzzaman M (2023) Bio-inspired sustainable synthesis of novel SnS2/biochar nanocomposite for adsorption coupled photodegradation of amoxicillin and congo red: effects of reaction parameters, and water matrices. J Environ Manage 334:117496. https://doi.org/10.1016/j.jenvman.2023.117496

Harja M, Buema G, Bucur D (2022a) Recent advances in removal of Congo Red dye by adsorption using an industrial waste. Sci Rep 12:1–18. https://doi.org/10.1038/s41598-022-10093-3

Harja M, Lupu N, Chiriac H, Herea DD, Buema G (2022b) Studies on the removal of Congo Red dye by an adsorbent based on Fly-Ash@Fe3O4 mixture. Magnetochemistry. https://doi.org/10.3390/magnetochemistry8100125

Hosseini SA, Vossoughi M, Mahmoodi NM, Sadrzadeh M (2019) Clay-based electrospun nanofibrous membranes for colored wastewater treatment. Appl Clay Sci 168:77–86. https://doi.org/10.1016/j.clay.2018.11.003

Jasim RA, Salman RH (2024) Congo red removal from aqueous solution by electrocoagulation- electro-oxidation combined system with Al and Cu–Mn–Ni nano composite as efficient electrodes. Case Stud Chem Environ Eng 9:100747. https://doi.org/10.1016/j.cscee.2024.100747

Kanmaz N, Yardimci B, Demircivi P (2025) In situ synthesis of MIL-125 on cinnamon stick and improved via carboxymethyl cellulose : A sustainable approach for super-high crystal violet adsorption. J Colloid Interface Sci 678:366–377. https://doi.org/10.1016/j.jcis.2024.09.035

Karadirek Ş, Tuna Ö, Simsek EB, Altuntas S, Cinar AY (2024) Facile fabrication of Ag decorated MnFeO 3 catalyst : comparative analysis of visible light driven antibiotic reduction and antibacterial performance. J Environ Manage 358:120891. https://doi.org/10.1016/j.jenvman.2024.120891

Katheresan V, Kansedo J, Lau SY (2018) Efficiency of various recent wastewater dye removal methods : a review. J Environ Chem Eng 6:4676–4697. https://doi.org/10.1016/j.jece.2018.06.060

Keshta BE, Gemeay AH, Sinha DK, Elsharkawy S, Hassan F, Rai N, Arora C (2024) State of the art on the magnetic iron oxide nanoparticles: synthesis, functionalization, and applications in wastewater treatment. Results Chem 7:101388. https://doi.org/10.1016/j.rechem.2024.101388

Lade H, Govindwar S, Paul D (2015) Mineralization and detoxification of the carcinogenic azo dye Congo red and real textile effluent by a polyurethane foam immobilized microbial consortium in an upflow column bioreactor. Int J Environ Res Public Health 12:6894–6918. https://doi.org/10.3390/ijerph120606894

Lafi R, Charradi K, Djebbi MA, Ben Haj Amara A, Hafiane A (2016) Adsorption study of Congo red dye from aqueous solution to Mg-Al-layered double hydroxide. Adv Powder Technol 27:232–237. https://doi.org/10.1016/j.apt.2015.12.004

Lu Y, Yu H, Zhu Y, Mu B, Wang A (2022) Recovering metal ions from oxalic acid leaching palygorskite-rich clay wastewater to fabricate layered mixed metal oxide/carbon composites for high-efficient removing Congo red. Chemosphere. https://doi.org/10.1016/j.chemosphere.2021.132543

Mahmoodi NM (2013) Photocatalytic degradation of dyes using carbon nanotube and titania nanoparticle. Water Air Soil Pollut. https://doi.org/10.1007/s11270-013-1612-3

Mahmoodi NM, Taghizadeh M, Taghizadeh A (2018) Mesoporous activated carbons of low-cost agricultural bio-wastes with high adsorption capacity: preparation and artificial neural network modeling of dye removal from single and multicomponent (binary and ternary) systems. J Mol Liq 269:217–228. https://doi.org/10.1016/j.molliq.2018.07.108

Mandal S, Calderon J, Marpu SB, Omary MA, Shi SQ (2021) Mesoporous activated carbon as a green adsorbent for the removal of heavy metals and Congo red: characterization, adsorption kinetics, and isotherm studies. J Contam Hydrol 243:103869. https://doi.org/10.1016/j.jconhyd.2021.103869

Marcelino RBP, Amorim CC (2019) Towards visible-light photocatalysis for environmental applications: band-gap engineering versus photons absorption—a review. Environ Sci Pollut Res Int 26:4155–4170. https://doi.org/10.1007/s11356-018-3117-5

Miao J, Zhao X, Zhang YX, Liu ZH (2021) Feasible synthesis of hierarchical porous MgAl-borate LDHs functionalized Fe3O4@SiO2 magnetic microspheres with excellent adsorption performance toward congo red and Cr(VI) pollutants. J Alloys Compd 861:157974. https://doi.org/10.1016/j.jallcom.2020.157974

Mohajershojaei K, Mahmoodi NM, Khosravi A (2015) Immobilization of laccase enzyme onto titania nanoparticle and decolorization of dyes from single and binary systems. Biotechnol Bioprocess Eng 20:109–116. https://doi.org/10.1007/s12257-014-0196-0

MohdAamir Khan GAB, Kuldeep, Yadav S, Singh N (2025) Enhanced adsorption of congo red dye using dried chitosan functionalized $MnFe_2O_4$ viscoelastic fluid. Colloids Surf A Physicochem Eng Asp. https://doi.org/10.1016/j.colsurfa.2025.136166

Muedi KL, Masindi V, Maree JP, Haneklaus N, Brink HG (2022) Effective adsorption of Congo Red from aqueous solution using Fe/Al di-metal nanostructured composite synthesised from Fe(III) and Al(III) recovered from real acid mine drainage. Nanomaterials. https://doi.org/10.3390/nano12050776

Oladoye PO, Adegboyega SA, Giwa ARA (2021) Remediation potentials of composite metal-organic frameworks (MOFs) for dyes as water contaminants: a comprehensive review of recent literatures. Environ Nanotechnol Monitor Manag 16:100568. https://doi.org/10.1016/j.enmm.2021.100568

Oladoye PO, Bamigboye MO, Ogunbiyi OD, Akano MT (2022a) Toxicity and decontamination strategies of Congo red dye. Groundw Sustain Dev 19:100844. https://doi.org/10.1016/j.gsd.2022.100844

Parimelazhagan V, Jeppu G, Rampal N (2022) Continuous fixed-bed column studies on congo red dye adsorption-desorption using free and immobilized nelumbo nucifera leaf adsorbent. Polymers (Basel). https://doi.org/10.3390/polym14010054

Pinheiro HN, Veloso FF, da Silva Abreu FOM, de Oliveira Almeida JLI, Cardial MRL (2023) Polysaccharides-based adsorbents for removal of Congo red dyes from wastewater. MOJ Ecol Environ Sci 8:138–141. https://doi.org/10.15406/mojes.2023.08.00283

Prabhakar N, Isloor AM, Padaki M, Fauzi Ismail A (2024) Fabrication of TiO2@ZIF-67 metal organic framework composite incorporated PVDF membranes for the removal of hazardous reactive black 5 and Congo red dyes from contaminated water. Chem Eng J 498:155270. https://doi.org/10.1016/j.cej.2024.155270

Rasilingwani TE, Gumbo JR, Masindi V, Foteinis S (2024) Removal of Congo red dye from industrial effluents using metal oxide-clay nanocomposites: insight into adsorption and precipitation mechanisms. Water Resour Ind. https://doi.org/10.1016/j.wri.2024.100253

Raval NP, Shah PU, Shah NK (2016) Adsorptive amputation of hazardous azo dye Congo red from wastewater: a critical review. Environ Sci Pollut Res Int 23:14810–14853. https://doi.org/10.1007/s11356-016-6970-0

Sachin, Singh N, Pramanik BK, Zizhou R, Houshyar S, Cole I, Yin H (2023) Fast and Effective Removal of Congo Red by Doped ZnO Nanoparticles. Nanomaterials. https://doi.org/10.3390/nano13030566

Şenyurt B, Akçamlı N, Ağaoğulları D (2021) In-situ synthesis of tungsten boride-carbide composite powders from WO3-B2O3–Mg–C quaternary system via a mechanochemical route. Ceram Int 47:1640–1650. https://doi.org/10.1016/j.ceramint.2020.08.280

Sharma G, AlGarni TS, Kumar PS, Bhogal S, Kumar A, Sharma S, Naushad M, ALOthman ZA, Stadler FJ (2021) Utilization of Ag2O–Al2O3–ZrO2 decorated onto rGO as adsorbent for the removal of Congo red from aqueous solution. Environ Res. https://doi.org/10.1016/j.envres.2021.111179

Singh KP, Wareppam B, Raghavendra KG, Singh NJ, de Oliveira AC, Garg VK, Ghosh S, Singh LH (2023) Heterophase grain boundary-rich superparamagnetic iron oxides/carbon composite for cationic crystal violet and anionic Congo red dye removal. Adv Eng Mater. https://doi.org/10.1002/adem.202300354

Sun W, Liu C, Liu S, Zhang J, Chen H, Qiu Z (2025) Effective adsorption of Congo red by an innovative biochar/LDH-derived MIL-100(Al): investigation of coexisting pollutants and mechanism

revelation. Sep Purif Technol 359:130670. https://doi.org/10.1016/j.seppur.2024.130670

Tehrani AD, Tahriri F, Najafabadi AK, Arefizadeh K (2024) Preparation of new green poly (amino amide) based on cellulose nanoparticles for adsorption of Congo red and its adaptive neuro-fuzzy modeling. Int J Biol Macromol 281:136287. https://doi.org/10.1016/j.ijbiomac.2024.136287

Xie J, Yamaguchi T, Oh JM (2021) Synthesis of a mesoporous Mg–Al–mixed metal oxide with P123 template for effective removal of Congo red via aggregation-driven adsorption. J Solid State Chem. https://doi.org/10.1016/j.jssc.2020.121758

Xu HY, Yang XW, Yu RP, Zuo T, Liu QY, Jia SP, Jia LY (2024) Adsorption properties of cellulose-derived hydrogel and magnetic hydrogels from *Sophora flavescens* on Cu2+ and Congo red. Int J Biol Macromol 274:133209. https://doi.org/10.1016/j.ijbiomac.2024.133209

Yardımcı B, Kanmaz N (2025) Ecosafe-design of carboxymethyl cellulose encapsulated polyphenolic bio-nanocomposite valorized for sustainable industrial textile dye removal. J Environ Chem Eng 13:115321. https://doi.org/10.1016/j.jece.2025.115321